Laplacian growth with separately controlled noise and anisotropy

M. G. Stepanov[1,2,*] and L. S. Levitov[3,4,†]
[1]*Institute of Automation and Electrometry, Novosibirsk, Russia*
[2]*Physics of Complex Systems, Weizmann Institute of Science, Rehovot, Israel*
[3]*Physics Department, Massachusetts Institute of Technology, Cambridge, Massachusetts*
[4]*Condensed Matter Physics, Weizmann Institute of Science, Rehovot, Israel*
(Received 25 May 2000; published 18 May 2001)

Conformal mapping models are used to study the competition of noise and anisotropy in Laplacian growth. For this purpose, a family of models is introduced with the noise level and directional anisotropy controlled independently. Fractalization is observed in both anisotropic growth and growth with varying noise. The fractal dimension is determined from the cluster size scaling with cluster area. For isotropic growth $d=1.7$, at both high and low noise. For anisotropic growth with reduced noise the dimension can be as low as $d=1.5$ and apparently is not universal. Also, we study the fluctuations of particle areas and observe, in agreement with previous studies, that exceptionally large particles may appear during growth, leading to pathologically irregular clusters. This difficulty is circumvented by using an acceptance window for particle areas.

DOI: 10.1103/PhysRevE.63.061102 PACS number(s): 05.40.−a, 61.43.Hv, 47.54.+r, 81.10.Aj

I. INTRODUCTION

In a large class of pattern-forming systems the growth is controlled by a Laplacian field. In diffusion limited aggregation (DLA) this field is the probability density of aggregating particles [1,2]. In viscous fingering it is pressure [3], and in crystal growth it can be either a diffusive or a thermal field [4]. After the DLA model was introduced by Witten and Sander [2], it became standard to simulate the Laplacian field by random walkers, which after being released at the periphery of the system diffuse toward the growing cluster and freeze on it. To simulate DLA, several numerical techniques have been developed, of which the most powerful are the off-lattice algorithms [5–7].

Applications to other Laplacian problems have been proposed based on the random walks idea. In particular, handling problems such as viscous fingering within this framework requires reducing the noise of individual walkers as well as modeling the surface tension. Reduction of noise was achieved by the method of multiple hits [8,9], in which particles freeze on a particular site adjacent to the already grown cluster only after this site has been visited more than $n_{\min}$ times, where $n_{\min}$ is an acceptance threshold. The method of noise reduction [8,9] was introduced in context of the on-lattice DLA models. More recently, this method was combined with the off-lattice technique and studied theoretically [10–12]. In an advanced version [10] of the multiple hits method the random walkers move off lattice and sticking rules are defined by using a finite number m of antennas attached to each particle, where, for instance, $m=4$ for square lattice DLA. Each of m antennas has a counter that scores the number of times n random walkers arrive on it and is then used to set a threshold $n_{\min}$ for freezing. Having a finite number of antennas used for each particle makes the sticking rules in the multiple hits model anisotropic. This anisotropy is essential because it is significantly amplified by the growth dynamics in the low noise regime of $n_{\min}\gg 1$. This built-in anisotropy of growth rules has been used to test the universality of DLA [13] and also to simulate dendritic crystal growth [14,10].

It has been proposed that surface tension can be modeled by introducing a probability $t<1$ of freezing upon each encounter with the cluster [15] or by making freezing dependent on the local neighbor configuration [16,9,17]. In the model [15] with $t\ll 1$ each randomly walking particle freezes only after encountering the cluster $t^{-1}\gg 1$ times. As a result, the freezing point is displaced from the point of first encounter by the distance $d\simeq t^{-1}$ in units of particle size. Effectively, in this model a finite length scale d is introduced over which the harmonic (Laplacian) measure describing the probability of the first encounter is probabilistically averaged. It was conjectured in Refs. [16,9,17] (and partially confirmed by various features observed in the growth patterns) that the length scale d simulates the capillary radius in the Laplacian problem with surface tension.

The field of Laplacian growth, despite being well developed by now, contains several long-standing unresolved problems. First, the lattice simulation, although extremely efficient algorithmically, does not seem to be a natural starting point for analytical understanding of large scale phenomena, such as fingering, fractalization, and scaling. Secondly, the methods of simulating Laplacian growth that have been used so far are not entirely free of problems, the most notable being an intrinsic anisotropy of growth rules. The original DLA rules [2] already use a square lattice and thus are anisotropic. This anisotropy is weak and reveals itself only in very large DLA clusters [5,7]. However, when the noise level is reduced using multiple hits, the underlying lattice anisotropy is amplified [18,11]. The noise-reduced growth remains vulnerable to anisotropy even when off-lattice random walks are used, due to the anisotropy of the freezing rules mentioned above.

*Email address: stepanov@iae.nsk.su
†Email address: levitov@mit.edu

It was demonstrated recently that Laplacian growth can be studied using an entirely different approach based on iterated conformal maps [19]. The model [19] uses analytical functions chosen in such a way that upon acting on a unit circle they produce bumps of prescribed size. Iterated n times with the parameter defining the bump size chosen according to a certain rule, these maps produce a cluster of n particles of nearly equal size. The conformal model of growth has recently become the subject of active work [20–25].

The goal of this article is to extend the conformal mapping methodology to problems with reduced noise and growth anisotropy. Here one clear advantage is that the growth rules using conformal mapping [19] are intrinsically *isotropic*. Because of that one can easily avoid problems pertinent to other models, in which growth anisotropy and reduced noise are intertwined. The main idea behind the noise reduction method proposed in this work is to average the Laplacian measure over a finite length that is larger than the particle size in the original model [19]. For that we alter the particle shape and use ''flat'' particles extended along the cluster boundary and thin in the growth direction. To compare our method of reducing noise to other techniques, we note that the positions of the flat particles are chosen strictly according to Laplacian measure, as in the multiple hits method [8,9]. The control over noise is achieved by suppressing noise at length scales shorter than the particle's larger dimension. This is in contrast with the multiple hits method, where noise is suppressed due to statistical averaging over many particle growth attempts uniformly over all length scales down to the particle size. Because of the appearance of this length scale our method somewhat resembles the surface tension models used in DLA lattice growth [15,16,9,17].

One notable difference from previous models is in the dependence of the computation time on the achieved level of noise reduction. Reducing statistical fluctuations in the multiple hits model required increasing the number of random walkers used to grow the cluster inversely with the noise reduction parameter. In our method one can reduce noise arbitrarily without increasing computation length, simply by varying the particle aspect ratio with particle areas kept fixed. We also demonstrate that growth anisotropy can be naturally incorporated in the conformal mapping method without affecting noise reduction.

Our plan in this article is as follows. We start by revisiting the conformal mapping model. We discuss some issues ignored before and propose a generalization to problems with reduced noise and anisotropy. In Sec. II we review the model, focusing on aspects that will be important in the rest of the article. In Sec. III we study the distribution of particle areas produced by the growth rules employed in Ref. [19]. We observe that these rules lead to the occasional appearance of very large particles. To fix this problem, we evaluate particle areas at each growth step and apply an acceptance criterion for newly grown particles according to their area. In Sec. IV we describe a model with reduced noise. To suppress noise we use particles that are thin in the growth direction and smooth at the corners. In Sec. V we show how these growth rules can be generalized for anisotropic growth. In Sec. VI we study the scaling properties of all introduced varieties of the model and compare them with each other. We find that the fractal dimension estimated from cluster radius scaling is less sensitive to noise than to anisotropy. For isotropic growth, both with and without noise reduction, the dimension is very close to 1.7. For anisotropic growth, reducing noise to the level at which anisotropy reveals itself strongly shifts the fractal dimension to somewhat lower values. In this regime, the fractal dimension depends on symmetry, and is found to be 1.62 for fourfold symmetry and 1.5 for threefold symmetry. Finally, in two Appendixes we discuss in detail the particle area distribution and possible improvements of our numerical procedure.

II. CONFORMAL MAPPING MODEL

We describe a growing cluster by a sequence of domains $\mathcal{D}_0 \subset \mathcal{D}_1 \subset \mathcal{D}_2 \subset \cdots$ corresponding to successive growth steps in time. In the canonical formulation [2], growth occurs due to particles diffusing from infinity one by one and freezing as soon as they reach the cluster boundary. The particle concentration $u(\mathbf{r})$ obeys the diffusion equation, which in the quasistationary approximation of slow growth is written as

$$\nabla^2 u(\mathbf{r}) = 0 \quad \text{with} \quad u(\mathbf{r}) = \begin{cases} 0, & \mathbf{r} \in \partial\mathcal{D}_{n-1} \\ \dfrac{1}{2\pi}\ln|\mathbf{r}|, & |\mathbf{r}| \to \infty. \end{cases} \tag{1}$$

The zero boundary condition on the cluster $\mathcal{D}_{n-1}$ describes freezing of the nth particle upon arrival with probability 1. The points of the cluster boundary $\partial\mathcal{D}_{n-1}$ where subsequent additions are made are selected randomly with probability given by the so-called harmonic measure

$$dP = |\nabla u|\, dl, \quad dl \subset \partial\mathcal{D}_{n-1}, \tag{2}$$

where dl is a boundary element of the cluster $\mathcal{D}_{n-1}$. As the domain changes, $\cdots \to \mathcal{D}_n \to \mathcal{D}_{n+1} \to \cdots$, the problem (1) has to be solved again for every new domain to determine from Eq. (2) the new particle position probability.

A considerable computational simplification of the problem can be achieved [19] by using a sequence of analytic functions $F_n(z)$, $n = 0,1,2,\ldots$, to represent the domains $\mathcal{D}_n$. The functions F_n are chosen so that each of them defines a conformal one-to-one mapping of the unit disk $|z| \leqslant 1$ on the domain $\mathcal{D}_n$, including the boundary. Adding a new object to the cluster at the nth growth step is described by changing the mapping F_n as follows:

$$F_n(z) = F_{n-1}(f_{\lambda_n,\theta_n}(z)), \quad F_0(z) = z. \tag{3}$$

Here the function $f_{\lambda_n,\theta_n}(z)$ maps the unit circle $|z| = 1$ onto a unit circle with a bump centered around the point $z = e^{i\theta_n}$ of the circle. The bump size is determined by the parameter λ_n as discussed below. The angle θ_n is chosen randomly at each growth step.

The key simplification that arises in the conformal mapping representation (3) is due to the fact that the harmonic measure (2) is translated into a uniform probability distribu-

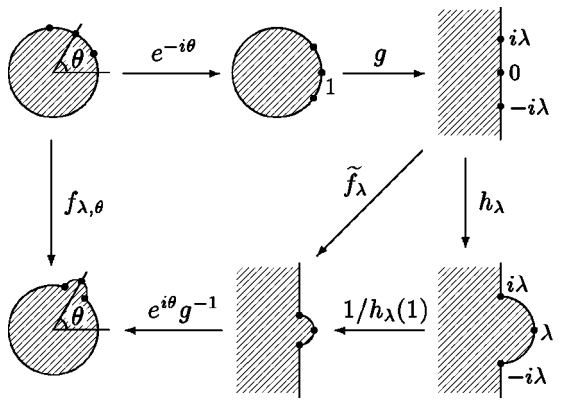

FIG. 1. The sequence of mappings constituting $f_{\lambda,\theta}(z)$ defined by Eqs. (4) and (5).

tion for θ_n, so that $dP(\theta)=d\theta/2\pi$. Also, there is no statistical correlation between subsequent θ's.

The form of the function $f_{\lambda,\theta}(z)$ growing the bumps can be chosen according to computational needs [19]. In this article we use

$$f_{\lambda,\theta}(z)=e^{i\theta}g^{-1}(\tilde{f}_\lambda(g(e^{-i\theta}z))), \tag{4}$$

where the function $g(z)=(z-1)/(z+1)$ maps the unit disk $|z|\leqslant 1$ onto the left half-plane $\mathrm{Re}\,z\leqslant 0$, and the function

$$\tilde{f}_\lambda(z)=h_\lambda(z)/h_\lambda(1),\quad h_\lambda(z)=z+\sqrt{z^2+\lambda^2}, \tag{5}$$

grows a semicircle of radius λ, as shown in Fig. 1. The function $\tilde{f}_\lambda(z)$ is defined in Eq. (5) so that $\tilde{f}_\lambda(1)=1$. This ensures that the mapping (4) maps $z=\infty$ onto itself.

Ideally, the values λ_n defining particle size should be chosen so that all particle areas are equal. In the conformal mapping model [19] this is approximately realized via predicting the bump size to be obtained at the nth step using the Jacobian of the already grown cluster mapping F_{n-1}.

The argument is as follows. The area of the semicircular bump grown using $\tilde{f}_{\lambda_n}(z)$ is $\pi\lambda_n^2[1+O(\lambda_n^2)]/8$. The area of the corresponding bump produced by $F_n(z)$, at small λ_n, is approximately $|J_{n-1}|^2\pi\lambda_n^2/2$, where J_{n-1} is the Jacobian of F_{n-1} evaluated at the position of the nth bump:

$$J_{n-1}=F'_{n-1}(z=e^{i\theta_n}). \tag{6}$$

Hence, to compensate for stretching due to the Jacobian J_{n-1}, one has to choose the values of λ_n as follows:

$$\lambda_n=|J_{n-1}|^{-1}\lambda_0, \tag{7}$$

where the parameter λ_0 defines particle size. For growth involving particles of very small size the rule (7) would have been sufficient to ensure identical areas of all bumps. For our problem, in which the bump sizes are small but finite, the areas are only approximately equal. However, one can demonstrate that, after certain improvements discussed in Sec. III, the rule (7) produces bumps with sufficiently close areas.

The form (4),(5) of the mapping $\tilde{f}$ has several nice features. First, since the fractional linear function $g(z)$ maps a circle onto a circle, the mapping $f_{\lambda,\theta}$ produces a crescent-shaped particle with circular boundary (see Fig. 1). Second, a simple calculation shows that the particle curvature radius equals λ. The latter has the following consequence. Consider growth starting from a circular cluster of radius r, described by the mapping $F(z)=rz$. The mapping $F(f_{\lambda,\theta}(z))$ then produces a particle of curvature radius equal to λr. After the value of λ is chosen according to the rule (7), $\lambda=\lambda_0/F'=\lambda_0/r$, the particle radius becomes equal to λ_0, independently of the cluster radius r. The area of this particle is readily evaluated:

$$a(\lambda_0,r)=a_*+\lambda_0 r-(r^2-\lambda_0^2)\tan^{-1}(\lambda_0/r),$$

$$a_*=\pi\lambda_0^2/2. \tag{8}$$

The area $a(\lambda_0,r)$ varies between a_* for $\lambda_0\ll r$ and $2a_*$ for $\lambda_0\gg r$. For a generic noncircular cluster the particle area cannot be found analytically. Statistics of the areas will be discussed in Sec. III. We will see that the typical area of a particle is of the order of a_*.

The overall size of the cluster $\mathcal{D}_n$ grown according to Eqs. (3) and (7) is well characterized [19] by the mapping F_n stretching factor at large scales:

$$R_n=F'_n(z\to\infty)=\prod_{k=1}^{n} f'_{\lambda_k,\theta_k}(z\to\infty). \tag{9}$$

The cluster radius R_n can be conveniently evaluated using Eq. (9) together with the property $g(\infty)=1$ as follows:

$$R_n=\prod_{k=1}^{n}[\tilde{f}'_{\lambda_k,\theta_k}(z=1)]^{-1}=\prod_{k=1}^{n}(1+\lambda_k^2)^{1/2}. \tag{10}$$

The reason for R_n to be an accurate measure of the cluster $\mathcal{D}_n$ radius lies in the properties of so-called univalent functions [19,21].

At large n the cluster radius R_n is expected to grow as n^α, where α is a numerical constant. This is consistent with Eq. (10) provided that $\lambda_n^2 n\to 2\alpha$ at large n [19,26]. The growth problem (1),(2) is believed to give rise to fractal objects with fractal dimension $d<2$. There are several conventional definitions of the fractal dimension of a growing cluster [1]. In this article we employ scaling of the cluster size with its area. Also, one can use box counting, or the relation between average growth velocity in a strip and the strip width.

Taking R_n defined in Eq. (9) as a cluster radius provides a numerically efficient method for calculating fractal dimension. For that one looks for a scaling relation of the form

$$R_n\propto A_n^{1/d}, \tag{11}$$

where A_n is the total area of the cluster $\mathcal{D}_n$. The dimension d is related to the parameter α describing scaling of λ_n as $d=\alpha^{-1}$, which is true provided $A_n\propto n$. In our simulation we make sure that individual particle areas have a sufficiently narrow distribution (see Sec. III), and thus the total cluster area is indeed proportional to the particle number.

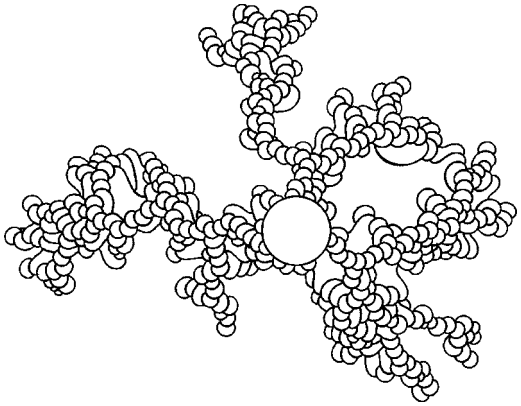

FIG. 2. Cluster of $N=400$ particles grown using the model (3),(7) with $\lambda_0=0.2$ and $f_{\lambda,\theta}$ of the form (4),(5). The boundary of each particle is displayed. Note large particles which appear rarely and seal fjords.

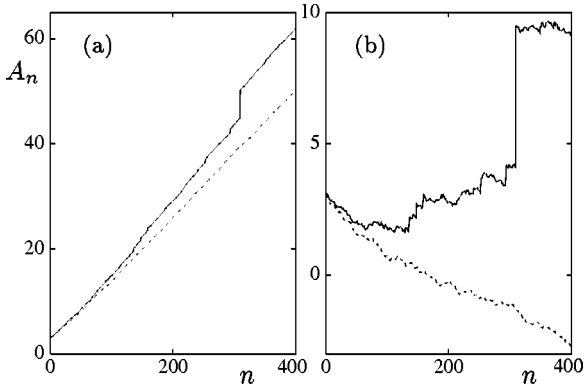

FIG. 3. (a) Solid line: total cluster area A_n dynamics for the growth of the cluster in Fig. 2, $N=400$, $\lambda_0=0.2$. Dotted line: the area A_n versus n for growth in which only particles with area inside the window $[0,3a_*]$ are accepted, other growth parameters are the same. (b) The same area dynamics as in (a) with a linear function subtracted: $A_n-2.1a_*n$ versus n.

Scaling properties of the growth problem described above have been explored by several groups [19–25]. It was concluded that the properties of growth resulting from the conformal mapping model match those of the lattice DLA models. Below we revisit the relation between the problem (1),(2) and the conformal mapping model (3),(4),(7) and discuss several interesting extensions of this model.

III. AREA DISTRIBUTION

In the earlier work [19] it was assumed that the rule (7) is sufficient to produce particles with nearly equal areas. This assumption was apparently consistent with the cluster images in which each particle is represented by one or few points. To investigate this issue more closely, in this work we have chosen a different method of representing particles, in which the exact boundary of each particle is shown. An example of a cluster with the boundaries of all individual particles displayed (see Fig. 2) demonstrates that the areas of almost all of the particles are indeed quite close. However, there are also a number of exceptional particles of large area.

Large particles tend to appear within fjords and seal the space between well developed branches. Typically, this happens when particle growth is attempted on the periphery of an actively growing region. Insufficiency of the rule (7) for keeping particle areas small is caused by fluctuations of the Jacobian $F_n'(z)$ over the unit circle $|z|=1$. These fluctuations can be large in magnitude and also very abrupt, happening on a scale of the order of λ_n within the circle arc mapped onto the particle boundary. In the case when a newly grown particle overlaps with such a fluctuation, it can be ''artificially stretched'' under the mapping.

The appearance of large particles was reported in Ref. [21] and a method for eliminating them was proposed, based on choosing an optimal shape of particles produced by the mapping $f_{\lambda,\theta}(z)$. It was argued [21] that the best value of the parameter $0<a<1$ in the mapping defined in Ref. [19] is given by $a=2/3$. This value provides a compromise between abundance of large particles at $a\to 0$ and a needlelike particle shape at $a\to 1$. Since in this article the particle shape will be used to tune noise, we employ a different method for eliminating large particles, as described below.

To study the role of exceptional particles, we calculate the particle areas generated by the growth model (3),(7). The method employed to evaluate particle areas is the following. For the particle grown at step n, we start with few points on the unit circle $|z|=1$ which are mapped by F_n on the particle boundary. Subsequently, we add new points on the circle $|z|=1$ between the old points, and compute distances between images of neighboring points under *all* mappings

$$f_n,\ f_{n-1}\circ f_n,\ \ldots,\ F_n=f_1\circ f_2\circ\cdots\circ f_n, \tag{12}$$

where f_k is a shorthand notation for f_{λ_k,θ_k} and $\circ$ stands for the mapping composition. We keep adding new points until the distances between the images of all neighbors will not exceed $\gamma\lambda_0$, where $\gamma\ll 1$ is a numerical factor. We used the above procedure with $\gamma=0.05$, which produces about 200–400 points per particle.

This method enables one to have an accurate graphical representation of each particle, as demonstrated in Fig. 2, and also to evaluate particle areas with an accuracy on the level of 0.1%. This is illustrated in Fig. 3(a) showing how the cluster total area A_n is changing during the growth of the cluster displayed in Fig. 2. The area A_n grows as a function of n in small steps of order $a_*=\pi\lambda_0^2/2$, alternating with occasional jumps of a much larger magnitude. The jumps correspond to the appearance of large particles which seal inner cluster regions. The decomposition of the growth of A_n into the smooth and singular parts is revealed more clearly in Fig. 3(b) showing the dependence of A_n versus n for the same growth as in Fig. 3(a), with a linear function $2.1a_*n$ subtracted.

A histogram of the individual particle areas $a_n=A_n-A_{n-1}$ is plotted in Fig. 4(a). The area distribution was obtained by averaging over 10 realizations of the first 1000 growth steps with the parameter $\lambda_0=0.2$ (the same as in Figs. 2 and 3). The area distribution $\mathcal{P}(a_n)$ is sharply peaked

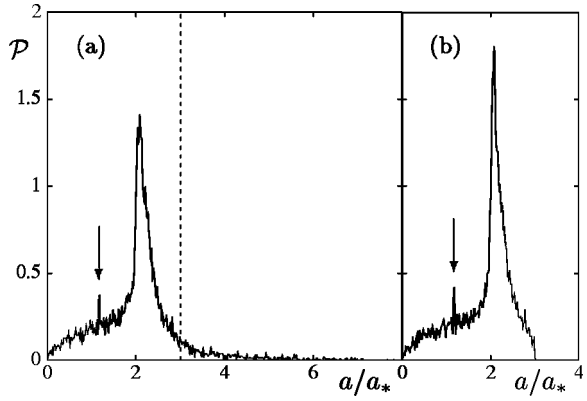

FIG. 4. (a) Probability distribution function of particle areas normalized by $a_* = \pi\lambda_0^2/2 \approx 0.063$ [see Eq. (8)]. Statistics were taken over 10 independent runs of the growth with $N=1000$, $\lambda_0 = 0.2$. Note the peak at $\sim 2.1a_*$ and the tail corresponding to exceptionally large particles. The largest area observed was $\approx 87.8a_*$ (see Fig. 2). Small peak marked by arrow is due to the primary particles growing directly on the unit circle. (b) Same as in (a) for growth in which only particles with areas in the window $[0,3a_*]$ are accepted.

about $2.1a_*$ and has a number of other interesting properties that will be discussed in Appendix A.

The feature of the distribution $\mathcal{P}(a_n)$ displayed in Fig. 4(a) that corresponds to the exceptionally large particles is the tail stretching far to the right from the main peak. Note that only the beginning of the tail is displayed in Fig. 4(a) because the weight of the tail in the probability distribution is insignificant, and so the values of $\mathcal{P}(a_n)$ far in the tail are too small to be visible on the scale of the peak.

To display the tail we replot the distribution $\mathcal{P}(a)$ on a log-log scale, as shown in Fig. 5. The right tail of $\mathcal{P}(a)$ is powerlike, $\mathcal{P}(a) \propto a^{-\mu}$ with $\mu \approx 2.5$. Since $\mu > 2$, the first moment $\langle a \rangle = \int a\mathcal{P}(a)da$ is finite (and thus $\langle a \rangle \simeq a_*$). However, since $\mu < 3$, the second moment of $\mathcal{P}(a)$ is divergent. The existence of the mean particle area $\langle a \rangle$ means that $\langle A_n \rangle \propto n$. However, the absence of variance implies that the

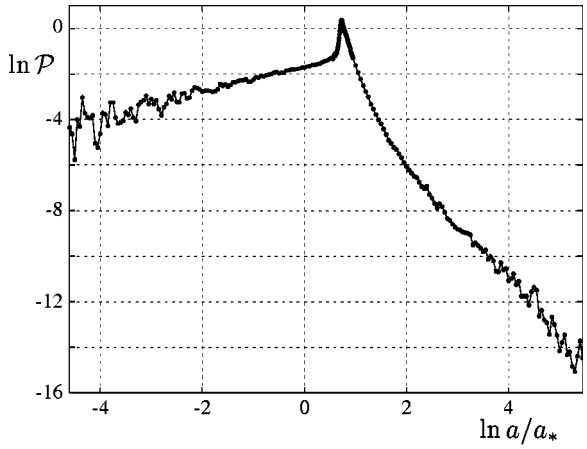

FIG. 5. Logarithm of the probability distribution function of particle area $\ln \mathcal{P}(a/a_*)$. Calculated from 83 realizations with $N = 2000$, $\lambda_0 = 0.8$.

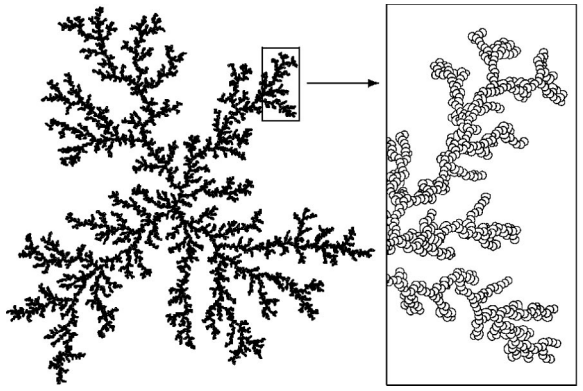

FIG. 6. Cluster grown with the particle area acceptance window $[0,3a_*]$ [see Fig. 4(b)], $N = 17\,545$, $\lambda_0 = 0.8$.

fluctuations of A_n about the mean value are non-Gaussian and larger than required by the central limit theorem. Both features are clear in the sample A_n dependence in Fig. 3.

Let us remark that the tail in Fig. 5 at its far end is apparently somewhat steeper than $a^{-\mu}$. We believe that this deviation from the $a^{-\mu}$ behavior is due to the finite number $N=2000$ of time steps in the growth samples used to obtain $\mathcal{P}(a)$. In a finite cluster there is an upper cutoff on possible particle areas. This makes the far tail of $\mathcal{P}(a)$ nonstationary, shifting the cutoff to larger areas as N increases.

Clearly, one would like to inhibit the appearance of large particles with areas in the tail of $\mathcal{P}(a)$. This is desirable because, even though the tail is quite thin and large particles are rare, extremely large particles appearing occasionally may affect macroscopic characteristics of the growth. In particular, the relatively slow power law decrease in the tail, $\mathcal{P}(a) \propto a^{-\mu}$, may affect the scaling of the cluster size R_n and/or the numerical accuracy of the scaling exponent. To eliminate the growth of large particles, we choose an acceptance threshold $a_{\max} = 3a_*$ to truncate the tail of the distribution in Fig. 4(a). Then, for each growth step, we calculate the new particle area a_n. The particle is accepted only if $a_n \leqslant a_{\max}$, otherwise the particle is discarded and a new attempt at particle growth is made. An example of the cluster grown according to these rules is displayed in Fig. 6.

One can see immediately that the overall structure of the branches in Fig. 6 is much more regular than that in Fig. 2. The distribution of areas for such a growth is shown in Fig. 4(b). Within the acceptance window $[0,a_{\max}]$ the distribution $\mathcal{P}(a)$ repeats in all details the distribution shown in Fig. 4(a) for the growth with all particle areas accepted.

For growth with large particles eliminated, the area A_n increases as a linear function of the step number. The average increment of A_n is given by the mean value of a_n taken from the distribution shown in Fig. 4(b). To verify this, we plot A_n versus n in Fig. 3 for the same growth parameters as those used in Fig. 2, where only the areas up to $3a_*$ are accepted. Note a small difference between the slope of the dependence at $n \leqslant 50$ and at larger n that appears because of relatively smaller size of the primary particles growing directly on the unit circle.

The growth model augmented with the area acceptance criterion has a new parameter $a_{\max}/a_*$. In principle, choos-

ing different values of $a_{\max}$ gives rise to different growth patterns. However, as long as the window $[0,a_{\max}]$ contains much of the $\mathcal{P}(a)$ peak area, we do not observe any qualitative change in the growth.

Scaling properties of the growth can be studied in several ways. Previous studies of scaling [19,21–24] are based on the relation $R_n \propto n^{\alpha}$, where R_n was obtained for the growth with unrestricted areas. However, it would be more in the spirit of the notion of a fractal to use the relation (11) between cluster size and its area. This clearly would not work well with large particles present, because statistical fluctuations of the cluster area A_n are quite large in this case. On the other hand, for the growth with restricted areas used in this work, the fluctuations of A_n are reduced to a level consistent with the central limit theorem, and thus one can employ the relation (11) to study scaling.

Of course, it is not clear *a priori* whether growth with area cutoff is equivalent macroscopically to growth with unrestricted areas. On general grounds, one may expect the growth to be significantly altered by eliminating large particles. Whether this is true can be indirectly tested by comparing the R_n vs n dependence for growth with unrestricted areas with the fractal dimension obtained from the relation (11) for growth with area cutoff. We note in that regard that the scaling exponent $d=1.7$ found below (see Sec. VI) matches exactly the value found in Ref. [19]. However, although the presence or absence of large particles seems to be irrelevant for the cluster size scaling, other growth characteristics, such as the structure of branches and fjords, are likely to be more sensitive to the method of treating large particles.

We postpone discussion of various details and features of the area distribution $\mathcal{P}(a)$ to Appendix A. In the remaining part of the article we use the conformal mapping model augmented with the area acceptance criterion to study several interesting Laplacian growth problems.

IV. NOISE-REDUCED LAPLACIAN GROWTH

Roughness of the growing cluster is mainly due to two factors: shot noise and the Mullins-Sekerka instability [27]. The shot noise results from the randomness of the aggregating particles' positions, and so it contributes to the fluctuations equally on all spatial scales down to the particle size. The Mullins-Sekerka instability is due to aggregation rate enhancement near the tips, which leads to incremental growth of perturbations of a smooth front. The wave-number dependence of the growth rate for a harmonic modulation of an interface moving with average velocity v is given by $\gamma_k = v|k|$. The linear k dependence of γ_k implies that the instability develops first on the smallest scale, in our problem given by the particle size.

To study the ultraviolet cutoff role, i.e., the effect of short distances on the noise and the instability, it is of interest to introduce a parameter in the problem that allows one to shift the value of the cutoff scale to values larger than the particle size. One expects that upon doing so both the noise and the instability growth rate will be reduced.

In the mapping model, the noise level can be controlled by altering the shape of aggregating particles. Below we show how by changing the function $\tilde{f}_{\lambda}(z)$, defined by Eq. (5), one can create ''flat'' particles that are wide along the interface and thin in the growth direction. The reason that noise is suppressed on using flat particles is the following. In this growth, a particular displacement of the growing cluster boundary amounts to a larger number of layers than in the case of rounded particles used in Ref. [19]. Then, due to statistical averaging over many particle layers the boundary displacement becomes less erratic, and so the noise is reduced. Quantitatively, the noise suppression factor can be estimated as the square root of the particle aspect ratio.

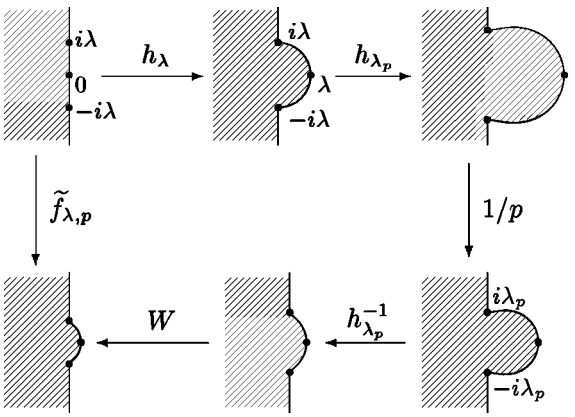

FIG. 7. The sequence of mappings constituting $\tilde{f}_{\lambda,p}(z)$ as defined by Eq. (13); $p=1.5$.

Flat particles can be produced by modifying $\tilde{f}_{\lambda}(z)$ as follows:

$$\tilde{f}_{\lambda,p}(z) = W h_{\lambda_p}^{-1}\left(\frac{1}{p} h_{\lambda_p}(h_\lambda(z))\right), \quad \lambda_p = \frac{2\lambda}{p+1/p}, \tag{13}$$

$$W = \left[h_{\lambda_p}^{-1}\left(\frac{1}{p} h_{\lambda_p}(h_\lambda(1))\right)\right]^{-1}, \quad p \geqslant 1. \tag{14}$$

The function $h_\lambda(z)$ is defined in Eq. (5), and its inverse has the form $h_\lambda^{-1}(z) = \frac{1}{2}(z-\lambda^2/z)$. The factor W is introduced in order to have $\tilde{f}_{\lambda,p}(1)=1$, as for the function $\tilde{f}_{\lambda}(z)$ defined by Eq. (5) above. The resulting function (4) satisfies $f_{\lambda,\theta}(\infty)=\infty$, which ensures the property $F_n(\infty)=\infty$ for all n.

The mapping produced by the function (13) is illustrated in Fig. 7. Note that, because of $h_{\lambda_p}(i\lambda)/p = i\lambda_p$, the square root singularities in $\tilde{f}_{\lambda,p}$ at $z=\pm i\lambda$ are absent for all $p>1$. Instead, the mapping composition (13) produces weaker singularities of the form $(z\pm i\lambda)^{3/2}$. This smooths the corners of the particles, as shown in Fig. 7.

Qualitatively, under variation of p the particle shape evolves as follows. At $p=1$ the mapping $\tilde{f}_{\lambda,p}$ form (13) coincides with Eq. (5). Increasing p produces particles with growing aspect ratio, as can be seen from comparing the enlarged parts of Figs. 10, 11, and 8 below.

To illustrate the effect of p on the particle shape, consider the mapping function (13) in the limit $p \gg 1$. First, one can rewrite Eq. (13) as

$$\tilde{f}_{\lambda,p}(z)=W'\left(h_\lambda(z)-\frac{\lambda_p^2(p^2-1)}{2h_{\lambda_p}(h_\lambda(z))}\right), \tag{15}$$

where W' is a prefactor chosen so that $\tilde{f}_{\lambda,p}(1)=1$. Expanding Eq. (15) to lowest order in $1/p$, one obtains

$$\tilde{f}_{\lambda,p}(z)=z+\frac{\lambda^2}{p^2}\left(\frac{z+2\sqrt{z^2+\lambda^2}}{(z+\sqrt{z^2+\lambda^2})^2}-Cz\right), \tag{16}$$

where $C=[2h_\lambda(1)-1]/h_\lambda^2(1)$ and h_λ is defined in Eq. (5). The boundary of the particle produced by $\tilde{f}_{\lambda,p}(z)$ of the form (16), to lowest order in $1/p$, is

$$x=\frac{2}{\lambda^2 p^2}(\lambda^2-y^2)^{3/2}, \tag{17}$$

where $x+iy=z$. The area of this particle is $3\pi\lambda^2/4p^2$. Mapped by g^{-1}, according to Eq. (4), the area is multiplied by a factor equal to 4 at $\lambda\ll 1$.

One can use the growth mapping model (3),(7) with the function (13) to grow clusters in much the same way as was done for the model with $p=1$ in Sec. III. The first step is to study the particle area distribution for growth with unrestricted areas. The distribution looks similar to that in Fig. 4, containing a central peak and tails corresponding to very large and very small particles. In this case the peak is somewhat wider than for the $p=1$ case. However, much of its weight in the distribution $\mathcal{P}(a)$ is still contained in the window $[0,3a_*]$. Here the ''standard area'' a_* is defined, by analogy with Eq. (8), as the area of a particle grown over a perfectly flat interface. [For $p\neq 1$ there is no closed form expression for the particle area, like Eq. (8), and so one has to calculate a_* numerically.]

As before, at each growth step we choose θ_n randomly, $0\leqslant\theta_n<2\pi$, and calculate the parameter λ_n using Eq. (7), i.e., based on the particle area predicted from the Jacobian J_{n-1}. Then we evaluate the actual area a_n of the particle. To inhibit the appearance of large particles, we use the acceptance window $[0,3a_*]$. If $a_n>3a_*$, the particle is not accepted and a new growth attempt is made.

An example of growth with $p=3$ and $\lambda_0=0.2$ is displayed in Fig. 8. In the inset we zoom in on the details of one finger. Note that individual particles are indeed quite flat and are evenly spread over the cluster boundary, indicating reduced noise. The growing interface is overall very smooth, without sharp tips or corners. Also, the fingers are much thicker than for the $p=1$ growth (see Fig. 6).

The cluster size R_n is defined by Eq. (9). As in Sec. III, the terms in the product (9) can be evaluated using the relation $f'_{\lambda_p,\theta}(\infty)=1/\tilde{f}'_{\lambda,p}(1)$, where

$$\tilde{f}'_{\lambda,p}(1)=\frac{h_\lambda(1)/\sqrt{1+\lambda^2}}{\sqrt{h_\lambda^2(1)+\lambda_p^2}}\,\frac{h_{\lambda_p}^2(h_\lambda(1))+p^2\lambda_p^2}{h_{\lambda_p}^2(h_\lambda(1))-p^2\lambda_p^2}. \tag{18}$$

In the following Sec. VI we use Eq. (18) along with Eq. (9) to evaluate the cluster radius R_n and study its scaling.

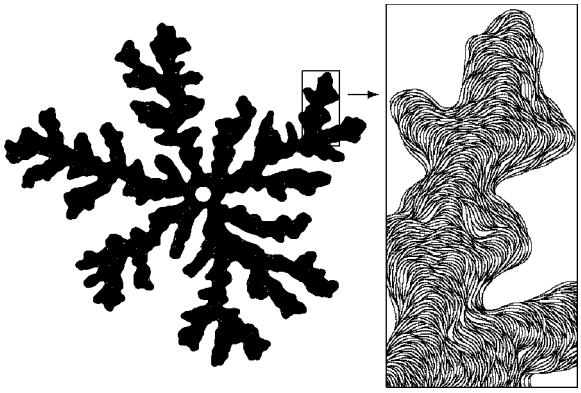

FIG. 8. Cluster grown with $p=3$, $\lambda_0=0.2$. The number of growth steps $N=15\,043$.

The appearance of the cluster in Fig. 8 shows that using flat particles indeed helps to reduce statistical fluctuations. In this model, effective averaging of the harmonic measure is due to the presence of a tangential-to-boundary length scale set by the particles' larger dimension. This length scale is controlled by the parameter p and becomes large at $p\gg 1$, if measured in units of the particle size $\sqrt{a_*}$. Noise reduction takes place due to the absence of fluctuations with wavelength smaller than the particles' larger dimension, resulting in a shift of the shot noise spectrum cutoff wave number from $2\pi/\sqrt{a_*}$ to lower values as the parameter p is increased. Because of reduced noise, as compared to the $p=1$ case, more aggregation events of flat particles are needed to reach a given radius of the cluster.

Averaging over a tangential length scale is somewhat similar to that used in the on-lattice DLA models to simulate surface tension [15,16,9,17]. In these works freezing of random walkers upon each encounter with the cluster was described by a finite probability $t<1$ which could be a function of occupancy of the sites around the freezing point. Since freezing of each particle typically takes place after about t^{-1} encounters with the cluster, at $t\ll 1$ these models are characterized by a large length scale over which the Laplacian measure is probabilistically averaged. Similarly, the flat particles used in our model can be thought of as the result of averaging over possible particle positions within a finite length scale taken over the harmonic measure. Moreover, there is a slight dependence of particle size on growth position: the particles appearing near the tips are somewhat smaller than those appearing in the concave regions (see Fig. 8). This correlation is consistent with the surface tension interpretation.

The crucial difference, however, is that particle positions in our model are chosen according to the unaltered harmonic measure, whereas in the surface tension models particle freezing depends on local boundary geometry. From that point of view our model is more similar to the multiple hits models [8,9] in which statistical averaging of the harmonic measure over particle growth attempts is used to control noise. In these models noise reduction is achieved by averaging over independent random walkers with a threshold on the minimal number of visits of each site required before freezing at this site. Since independent walkers arrive at very

distant points of the cluster boundary, this averaging is not characterized by an additional large length scale and thus bears no resemblance to surface tension.

The models using finite freezing probability $t<1$ have been shown to give rise to clusters with thick branches. The Laplacian character of the dynamics and the analogy of the averaging length scale with the capillary radius has been pointed out [15] and a relation with the Saffman-Taylor problem with surface tension has been conjectured [17]. Because of the large length scale appearing in our averaging scheme, here a similar relation to the problems with surface tension can be conjectured. Indeed, the growth displayed in Fig. 8 looks like a typical fingering pattern observed in the Saffman-Taylor problem with surface tension. As a word of caution, one should realize that all available evidence for the equivalence between the problem with surface tension and our large p growth, however similar they appear to be, is rather indirect. The issue of whether or not this growth model is indeed characterized by an effective surface tension and how the latter compares to the noise will be discussed elsewhere.

V. ANISOTROPIC GROWTH MODEL

The iterated mapping model (3),(7) can be generalized to describe spatial anisotropy of the local growth rate. Such anisotropy is characteristic of crystal growth, in which all particles arriving at the crystal-liquid interface have to accommodate to the anisotropic crystal structure [4].

Anisotropic growth often gives rise to anisotropic irregular fingering patterns called dendrites [16,14,18,10]. The dynamics of dendrite growth obeys scaling laws similar to that of isotropic Laplacian growth [7,28]. One of the outstanding theoretical questions is how the scaling exponents depend on the anisotropy.

In this problem, the cluster grows due to spatially isotropic diffusion and aggregation of particles. Thus the quasistationary probability distribution still obeys Eq. (1). The difference from the isotropic model is that the cluster change due to particle freezing at the boundary depends on the local growth direction $\mathbf{v}$, $|\mathbf{v}|=1$. (The unit vector $\mathbf{v}$ is normal to the boundary.) Accordingly, the probability of joining the cluster becomes a function of $\mathbf{v}$, and Eq. (2) is replaced by

$$dP=\Omega(\mathbf{v})\,|\nabla u|\,dl,\quad dl\subset\mathcal{D}_{n-1}, \tag{19}$$

where the function $\Omega(\mathbf{v})$ describes anisotropy.

In order to include anisotropy in the mapping model (3),(7), at the nth growth step one has to be able to predict the local growth direction $\mathbf{v}_n$ from particle positions described by randomly chosen angles θ_k, $k=1,2,\ldots,n-1$. This is possible because the complex-valued Jacobian of a conformal mapping keeps track of the angle change under the mapping. Specifically, consider $\Theta_n=\theta_n+\arg J_{n-1}$, where J_{n-1} is given by Eq. (6). Then Θ_n defines a normal to the cluster boundary, $\mathbf{v}_n=\cos\Theta_n\hat{x}+\sin\Theta_n\hat{y}$, at the growth point $F_{n-1}(e^{i\theta_n})$.

Now, there are several possible ways to account for the growth anisotropy. For instance, one can introduce the anisotropy by making λ_n a function of Θ_n, e.g., $\lambda_n\propto\Omega^{1/2}(\mathbf{v}_n)$. Another way is to introduce an acceptance probability for the particles that depends on Θ_n in some way. In the simulations reported below we use an acceptance window for $M\Theta_n$ with $M=3,4,\ldots$, corresponding to growth with M-fold symmetry. Only particles with Θ_n such that

$$-\theta_{\max}\leqslant M\Theta_n\leqslant\theta_{\max} \tag{20}$$

are accepted. Here $\theta_{\max}$ is a parameter in the interval $[0,\pi]$ controlling the degree of anisotropy. Small values of $\theta_{\max}\ll\pi$ correspond to highly anisotropic growth, whereas fully isotropic growth is recovered in the limit $\theta_{\max}\to\pi$.

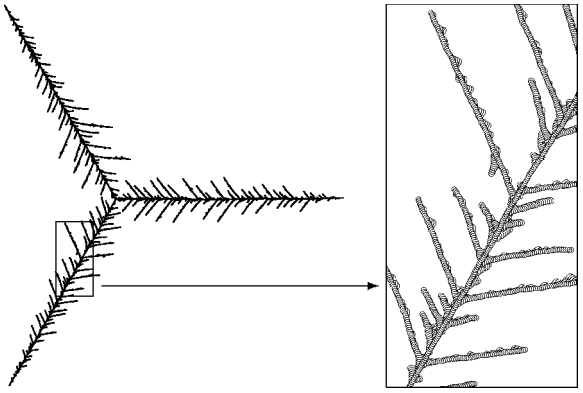

FIG. 9. Anisotropic growth with $M=3$ obtained using the window (20) for the growth direction with $\cos\theta_{\max}=0.9$. Other parameters used: $N=10\,146$, $\lambda_0=0.8$, $p=1.5$.

Other aspects of the simulation are the same as in Sec. IV. We employed the elementary mapping $\tilde{f}_{\lambda,p}(z)$ of the form (13) with the noise level controlled by the parameter $p\geqslant 1$. Particles with large areas were eliminated using the acceptance window $[0,3a_*]$ defined in Sec. IV. An example of growth with threefold symmetry ($M=3$) is shown in Fig. 9. In this case, we used $\lambda_0=0.8$, $p=1.5$, and $\theta_{\max}=\cos^{-1}(0.9)\approx 0.451$. The cluster is characterized by overall symmetric main branches covered with numerous sidebranches.

In our model one has separate control over the degree of anisotropy and over noise, via the parameters $\theta_{\max}$ and p. This is convenient for studying the effects of noise on the ordering of branches in dendrites. To illustrate that, we compare two growths with fourfold symmetry, displayed in Figs. 10 and 11. The cluster in Fig. 10 is obtained using the $p=1$ model without noise reduction, as described in Secs. II and III. The cluster in Fig. 11 is grown using the noise reduced model of Sec. IV with the parameter $p=2$. In both cases, we use the same anisotropy parameter: $\theta_{\max}=\cos^{-1}(0.95)\approx 0.318$. One notes high anisotropy of the growth present at small scales in both cases, which is significantly suppressed at larger scales for the noisy growth with $p=1$ (see Fig. 10). However, the $p=2$ growth with low noise remains very anisotropic at all scales (see Fig. 11).

It is known from studies of on-lattice DLA models that noise, no matter how strong, gives way to anisotropy at sufficiently large scales [5,6,18,11]. We thus expect that a simi-

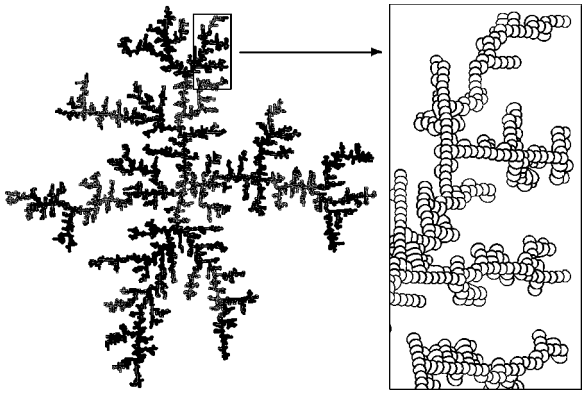

FIG. 10. Anisotropic growth with $M=4$, $\cos\theta_{\max}=0.95$, and high noise: $p=1$, $N=7635$, $\lambda_0=0.3$.

lar effect may take place in the noisy growth with $p=1$, making the growth shown in Fig. 10 at larger scales look like that in Fig. 11.

In agreement with the studies of off-lattice DLA models [14], we observed that dendritic growth with the symmetry of order $M=3,4$ is much more stable with respect to noise than that with $M=5,6$ or higher. The scaling properties of anisotropic growth will be studied in Sec. VI.

VI. SCALING PROPERTIES

Scaling of R_n for all growth models introduced above is studied here using the following procedure. The cluster radius R_n obtained from Eqs. (9), (10), and (18) is plotted against the cluster area A_n, evaluated as the sum of individual particle areas a_n. Asymptotically, at large n, one has $R_n \propto A_n^{1/d}$. To determine d more accurately we optimize initial conditions of the growth, represented in our model by the nondimensionalized particle size λ_0, as described below.

In the log-log plot of R_n versus A_n one can clearly distinguish two regimes, initial growth and developed or *regular* growth, characterized by somewhat different slopes of the corresponding parts of the $\ln R$ vs $\ln A$ curves. The geometrical meaning of these regimes is as follows. For isotropic growth, with or without noise suppression, the cluster initially consists of branches growing essentially independently. Later, at the regular growth stage, the number of main branches is reduced to four or five, all interacting and competing with each other. For anisotropic growth with M-fold symmetry the number of main branches is M at all stages of growth. Regular growth in this case is distinguished by many fingers appearing on the sides of M main branches.

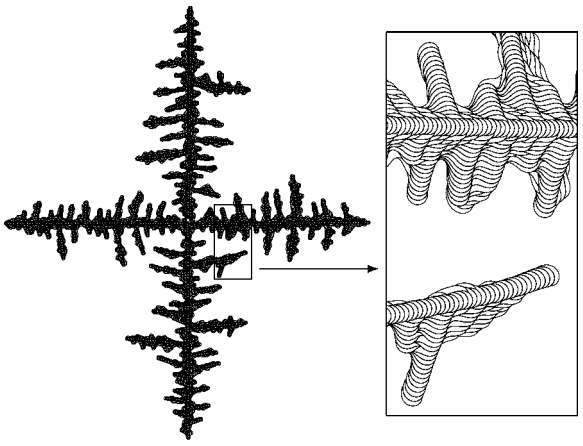

FIG. 11. Anisotropic growth with $M=4$, $\cos\theta_{\max}=0.95$, and low noise: $p=2$, $N=6782$, $\lambda_0=0.8$.

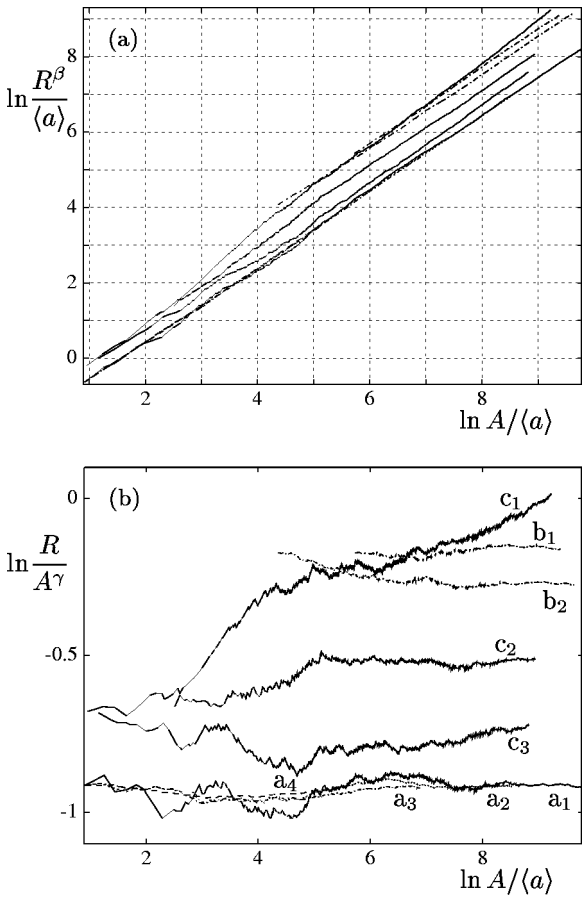

FIG. 12. Log-log plots of $R^\beta/\langle a\rangle$ (a) and R/A^γ (b) vs normalized area $A/\langle a\rangle$ for several clusters described in the text. Here $\beta=1.7$, $\gamma=1/1.7=1/\beta$, and $\langle a\rangle$ is the particle area averaged over the cluster. The plots (a) and (b) are connected by an affine transformation.

The initial stage is more pronounced when the particle size, determined by the value of λ_0, is much smaller than the unit circle from which the growth starts. Since we are interested in regular growth scaling, in each case studied we tried to optimize the value of λ_0 to shorten the initial growth stage, carefully checking that the variation of λ_0 has no detectable effect on the asymptotic slope of the $\ln R$ vs $\ln A$ curve. The benefit of shortening the initial growth stage is that, at a constant number of particles, it leads to longer regular growth and thus allows one to extract the scaling exponent with higher precision. The resulting curves are presented in Fig. 12, as described in the figure caption and below.

The optimal value of λ_0 determined for the isotropic growth with $p=1$ is close to $\lambda_0=0.8$. For the scaling analy-

sis we used the growth displayed in Fig. 6, in which $N=17\,545$, $\lambda_0=0.8$, and $p=1$. In Fig. 12, it corresponds to the lowest of the curves, marked by a_1. To eliminate the effect of fluctuations at the initial stage of the growth, we also generated the curves a_2, a_3, and a_4, by averaging $\ln R$ over 5, 10, and 50 growth realizations with $N=5000$, 1000, and 200 time steps, respectively.

For isotropic growth with reduced noise we analyzed two growths with $p=3$: curve b_1 with $N=11\,611$, $\lambda_0=0.1$; curve b_2 with $N=15\,043$, $\lambda_0=0.2$. The curve b_2 corresponds to the growth displayed in Fig. 8. At low noise, the fluctuations of R_n are quite small, which makes additional averaging over realizations unnecessary.

Note that for the isotropic growth models the strategy of optimizing λ_0 works quite well, allowing one to almost entirely eliminate the initial growth region. The scaling dimension found from the slope of the best straight line fits is close to 1.7. To study the deviation from 1.7, we subtract from all curves the linear function $\ln R=\ln A/1.7$ and plot the result in the lower part of Fig. 12. Note that upon this subtraction the curves for isotropic growth, with or without noise suppression, become nearly perfectly horizontal. Estimate of the deviation from the best horizontal line fit shows that the value 1.7 is accurate within 1%.

For anisotropic models, we consider three different growths: curve c_1 with $N=10\,146$, $\lambda_0=0.8$, $p=1.5$, $M=3$; curve c_2 with $N=7635$, $\lambda_0=0.3$, $p=1$, $M=4$; curve c_3 with $N=6782$, $\lambda_0=0.8$, $p=2$, $M=4$. These curves correspond to the growths displayed in Figs. 9, 10, and 11, respectively. As above, we subtract the linear function $\ln R=\ln A/1.7$. However, after this subtraction, the curves c_1 and c_3 retain some residual slope. Estimating it, we conclude that the best value for the fractal dimension is $d\approx 1.5$ for curve c_1 and $d\approx 1.62$ for curve c_3. The latter value agrees with the values $d\approx 1.58$ and $d\approx 1.63$ for growth with $M=4$ reported in Refs. [28,7].

For the curve c_2 corresponding to anisotropic growth with noise, after subtracting $\ln R=\ln A/1.7$, we do not find any significant residual slope. It is possible, however, that the dimension 1.7 corresponds to the crossover regime and changes to a lower value at larger N. Similar behavior is known to take place in on-lattice DLA growth [7], where the dimension 1.7 observed for not very large clusters crosses over to 1.63 at $N\sim 4\times 10^6$.

To understand possible sources of errors in determining the fractal dimension from $\ln R$ vs $\ln A$ curves, here we consider how R_n and A_n fluctuate with n. The fluctuations of $\ln R_n$ gradually decrease with increasing n, as can be clearly seen in Fig. 12(b). A convenient way to analyze fluctuations is to plot pairs $(\ln R_N,\ln A_N)$ for particular N, repeating growth many times. In Fig. 13 we present results for 10^3 growth samples and several values of N. The resulting clouds become more compact as N increases, indicating that the fluctuations of $\ln R_N$ and $\ln A_N$ are decreasing.

Let us first discuss fluctuations of $\ln A_n$. The total area A_n is the sum of individual particle areas a_k, $k=1,2,\ldots,n$. Assuming that the areas a_k are independent or, more precisely, have only short correlations, one obtains a Gaussian

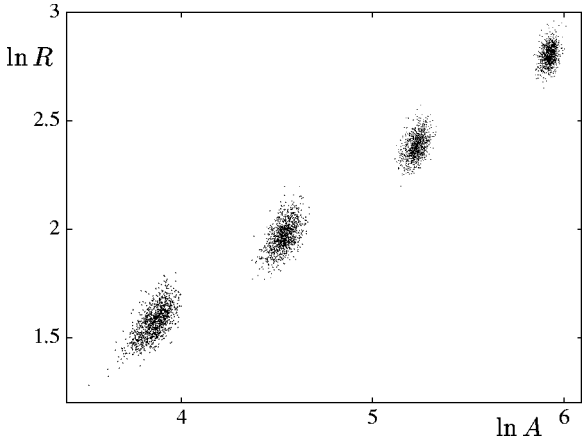

FIG. 13. Clouds of points $(\ln R,\ln A)$ corresponding to 1000 realizations for $N=25$, 50, 100, and 200, $\lambda_0=0.8$, $p=1$.

distribution with the variance $\propto n$. (As we argue below, there exist long negative correlations of particle areas, which may further reduce fluctuations of A_n.) The fluctuations of $\ln A_n$ are simply given by relative fluctuations $\delta A_n/A_n$, which means that for large n the distribution of $\ln A_n$ is also Gaussian, with the variance proportional to n^{-1}.

On the other hand, the radius R_n is a *product* (9) of stretching factors $J_k^{(\infty)}=f_k'(z\to\infty)$. Since $J_k^{(\infty)}>1$ for all k, the quantity R_n grows monotonically, so that $R_n\propto A_n^{1/d}$ at large n. Thus the noise due to fluctuations of $J_k^{(\infty)}$ is of a multiplicative nature. One can write

$$\ln R_n=\sum_{k=1}^{n}\ln f_k'(z\to\infty), \tag{21}$$

which suggests that the distribution of $\ln R_n$ is Gaussian, i.e., the distribution of R_n is log-normal. Indeed, the log-normal fit perfectly describes the statistics of R_n, as demonstrated in Fig. 14. However, attempting a Gaussian fit produces an asymmetric distribution deviating from the observed distribution of $\ln R_n$. Thus, even though the relative fluctuations of R_n are small, the statistics is best described as log-normal.

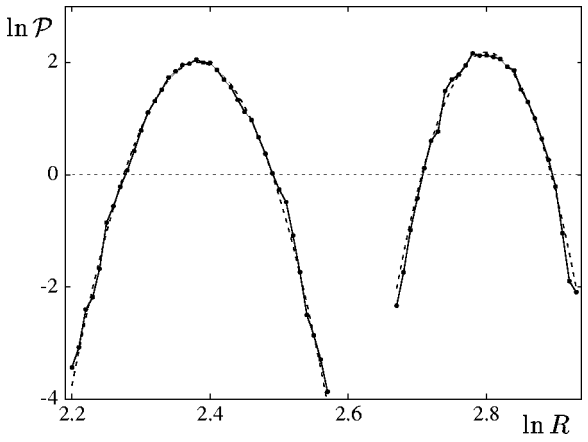

FIG. 14. Probability distribution of $\ln R$ for $N=100$ and $N=200$ calculated from 10 368 and 2862 growth realizations, respectively; $\lambda_0=0.8$, $p=1$.

Naively, Eq. (21) implies growth of the variance of $\ln R_n$ with increasing n. However, Figs. 13 and 14 demonstrate that, on the contrary, the width of the $\ln R_n$ distribution is decreasing with increasing n. This nontrivial behavior was first mentioned, without explanation, in Ref. [21].

To rationalize the observed sharpening of the distribution of R_n, one can argue as follows. We note that the dynamics of R_n is characterized by a negative feedback. Consider growth of a cluster that at the nth step has a radius smaller than average. Then the Jacobian of F_n is typically smaller than its mean value at this number of particles. In this case, according to Eq. (7), subsequently growing particles will have larger λ_k's, and thus larger areas, until the cluster radius approaches the average value. The evolution of a cluster that at a certain step has a radius larger than average can be considered in a similar way. This long time anticorrelation of λ_k's suppresses the fluctuations of R_n. It also produces long negative correlations of particle areas.

VII. SUMMARY

To conclude, growth models using conformal mappings have large flexibility allowing for independent control over noise and growth anisotropy. We generalized the model [19] by using flat particles to suppress noise. It is essential that these models lead to intrinsically isotropic growth with reduced noise, in contrast with other previously studied models. Also, we demostrated that favoring growth in certain directions can be used to simulate anisotropy of the growth rate.

Having separate control of the noise and anisotropy, we have been able to analyze their effects on scaling properties. We found that the fractal dimension $d=1.7$ universally for any isotropic growth, regardless of the noise level. However, the fractal dimension is somewhat reduced in the presence of anisotropy.

It was assumed [19] that particle size fluctuations, present in the conformal mapping model, are insignificant. We observed that the growth rules used in Ref. [19] lead to the occasional appearance of exceptionally large particles. We have shown that by augmenting the model with an area acceptance criterion this problem is fixed.

Clearly, more work has to be done to establish the relation of the models introduced with real physical processes, like viscous fingering or dendritic crystal growth. Another interesting open question is how to introduce an effective surface tension.

ACKNOWLEDGMENTS

We thank G. E. Falkovich, M. B. Hastings, V. A. Kazakov, V. V. Lebedev, B. Z. Spivak, and P. B. Wiegmann for useful discussions. The hospitality of the Weizmann Institute made our collaboration possible. This work was partially supported by the Minerva Foundation (M.S.).

APPENDIX A: DETAILS OF THE PARTICLE AREA DISTRIBUTION

Here we discuss in more detail the distribution of particle areas. The main feature manifest in the area histogram plotted in Fig. 4 is a sharp asymmetric peak at $\approx 2.1 a_*$. This peak has its origin in the dependence of particle size on the growth point.

The argument is as follows. First we note that the growth is taking place predominantly at the tips of the branches. Because of that, for several particles growing on each other, there is a tendency to preserve growth direction. This leads to formation of relatively long chains of particles growing in a particular direction, clearly seen in the inset of Fig. 6. The chains are mostly formed at the tips of outer branches.

Now, consider a particle growing near one of the tips. The area of this particle has some dependence on the position of the growth point relative to the tip. The peak in the histogram in Fig. 4 is explained if one assumes that the particle area has a local minimum in the forward growth direction. The minimum in the area leads to a caustic in the histogram. Ideally, this would produce an asymmetric square root singularity with probability equal to zero on the left side. Because of particle size variation among branches, the singularity is smeared into a peak.

To verify the above assumption, we consider the areas for the first few particles grown on the $|z|=1$ circle with the parameter $\lambda_0=0.2$. The area of the very first particle is close to $1.2a_*$ and, according to Eq. (8), is independent of its position. The area of the second particle a_2 depends on its position θ relative to the first particle, as shown by the solid line in Fig. 15(a). Note that the area is the same as that of the first particle when the particles are far apart, $\theta \gg \lambda_0$, and is overall substantially larger when the particle overlap $\theta \sim \lambda_0$. Partially, this is explained by the dependence (8) of particle area on the circle radius [assuming that $a_2(\theta \sim \lambda_0)$ can be crudely estimated by Eq. (8) with $r=\lambda_0$.] Another effect that contributes to the area a_2 increase for $\theta \sim \lambda_0$ is the variation of the Jacobian as a function of θ, leading to additional stretching of the second particle.

The feature in Fig. 15(a) that is of interest in connection with the peak in the area distribution $\mathcal{P}(a)$ is the minimum of $a_2(\theta)$ at $\theta=0$. Translated to the histogram of areas, it leads to a caustic described by a square root singularity. However, as a possible explanation of the peak in Fig. 4 this is only partially satisfying, since one has to understand why similar caustics due to the two maxima of $a_2(\theta)$ are not observed in Fig. 4.

The reason for the difference between the effects of maxima and minima can be seen from a comparison with the cases of three and four particles. Consider the situation when the second particle is centered exactly on the first particle, and the third particle is grown at an angular position θ relative to the first two particles. The area of the third particle $a_3(\theta)$ is plotted in Fig. 15(a) as the dashed line. Note that, since the curvature at the minimum of $a_3(\theta)$ at $\theta=0$ is much smaller than for $a_2(\theta)$, the corresponding caustic in $\mathcal{P}(a)$ will be much stronger. On the other hand, the curvature at the maxima of $a_3(\theta)$ is about the same as that for $a_2(\theta)$.

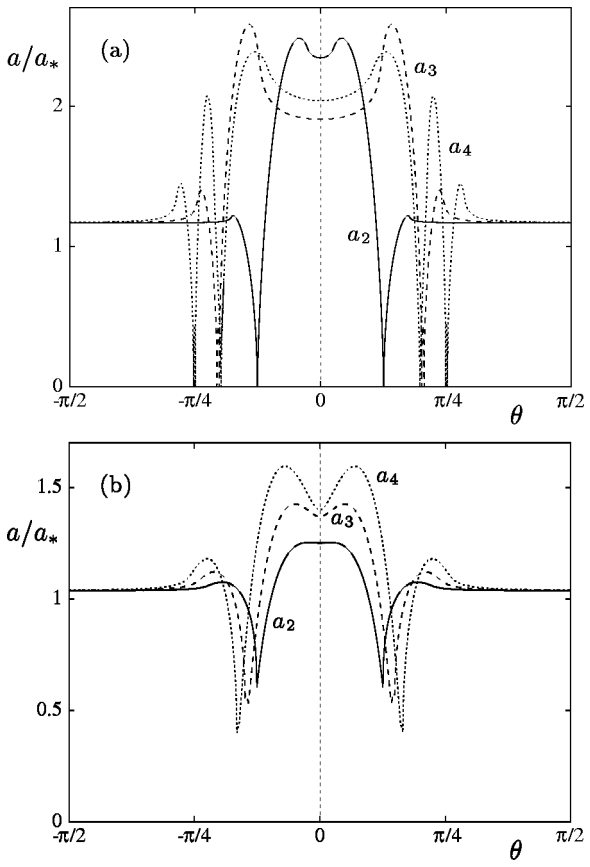

FIG. 15. Area of a particle as a function of its growth point, characterized by θ.

Both observations remain correct for any number of particles. To illustrate this we plot the area $a_4(\theta)$ of the fourth particle in the presence of three particles grown exactly on top of each other—see the dotted line in Fig. 15(a).

Another notable feature in the plots of $a_{2,3,4}(\theta)$ is that the area becomes much smaller than a_*, approaching zero near certain values of θ. This behavior is related to growth near particle corners, which are the points of divergence of the Jacobian. According to Eq. (7), a larger Jacobian translates into a smaller particle area. The particles growing near corners form the tail of the area distribution $\mathcal{P}(a)$ at small areas $a \ll a_*$. The behavior of $\mathcal{P}(a)$ in this tail, $\mathcal{P}(a) \propto a^{1/2}$, follows from the square root divergence of the Jacobian at particle corners. The slope 1/2 is clearly seen in the $\ln \mathcal{P}$ vs $\ln a$ plot in Fig. 5.

The features in $a_{2,3,4}(\theta)$ discussed above evolve in an interesting way for models with lower noise corresponding to $p>1$—see Fig. 15(b). The plots of $a_{2,3,4}(\theta)$ in this figure are produced for the model with $\lambda_0=0.2$ and $p=3$ in the same way as above for $p=1$. Note that relative changes of the area as a function of θ are smaller than for $p=1$. One reason for this is the weaker curvature variation for flat particles, which makes the particle area less sensitive to the growth point position. Another reason is that at $p>1$ the particle corners have no cusps, and thus particles with small areas do not appear.

APPENDIX B: DISCUSSION OF THE NUMERICAL METHOD

Here we comment on the optimal choice of the numerical procedure. First, since the areas of new particles are evaluated before the particles are accepted, one could, instead of eliminating large particles, change the growth algorithm so that all particle areas become equal. This can be achieved by adjusting the parameter λ_n for each particle until its area converges to a given value. Although this would somewhat slow down the speed of computation, an obvious gain would be in a more direct relation with the standard DLA growth.

Also, one could attempt to increase the speed and efficiency of the growth algorithm by introducing in it various improvements.

(i) Coarsening of the mappings that correspond to particles sufficiently deep in the stagnation regions. It was demonstrated in Ref. [19] that an accurate envelope of the cluster can be obtained by using a truncated Laurent series for $F_n(z)$. One can implement this observation as follows. At the growth step n choose some $1<m<n$ in such a way that all particles with the numbers $\leqslant m$ are located sufficiently deep inside the stagnation part of the cluster. Then one can replace the mapping $F_n=f_1\circ\cdots\circ f_n$ by

$$F_n^{(\mathrm{approx})}=[f_1\circ\cdots\circ f_m]_{\mathrm{truncated}}\circ f_{m+1}\circ\cdots\circ f_n, \qquad \text{(B1)}$$

where the mapping in brackets that is replaced by truncated series is nothing but F_m. One can choose m so that the finite series representation of the mapping $F_m(z)$ is accurate for z in the active growth region. By this trick, instead of computing a composition of n functions, one has to deal with only $n-m$ functions at each growth step. Since at large n most of the particles are in the stagnation regions, one may have $n-m \ll n$.

(ii) Evaluating the particle area with lower precision. We used several hundred points on each particle's boundary, which produces areas accurate within 0.1%. In practice, such a high precision may not be necessary. Instead, one can predict particle areas by estimating the Jacobian at several points chosen within the bump according to some rule or randomly.

(iii) Using an area acceptance window to discriminate against very small particles with areas $\ll a_*$. These particles essentially do not change the structure of the cluster branches, except near the corners between adjacent particles. However, due to the presence of small particles additional mappings appear in the composition sequence $f_n\circ\cdots\circ f_1$, which slows down the computation.

We have not used these procedures in the simulations described above nor have we systematically studied their efficiency. We felt that, at the initial stage, keeping the growth algorithm as precise and simple as possible, even at the price of somewhat slowing it down, makes the results more solid.

[1] A. Erzan, L. Pietronero, and A. Vespignani, Rev. Mod. Phys. **67**, 545 (1995); T. Vicsek, *Fractal Growth Phenomena* (World Scientific, Singapore, 1992); *On Growth and Form: Fractal and Non-Fractal Patterns in Physics*, edited by H.E. Stanley and N. Ostrowsky (Martinus Nijhoff, Dordrecht, 1986).
[2] T.A. Witten and L.M. Sander, Phys. Rev. Lett. **47**, 1400 (1981).
[3] D. Bensimon, L.P. Kadanoff, S. Liang, B.I. Shraiman, and C. Tang, Rev. Mod. Phys. **58**, 977 (1986).
[4] J.S. Langer, Rev. Mod. Phys. **52**, 1 (1980).
[5] R.C. Ball and R.M. Brady, J. Phys. A **18**, L809 (1985).
[6] P. Meakin, J. Phys. A **18**, L661 (1985).
[7] P. Meakin, R.C. Ball, P. Ramanlal, and L.M. Sander, Phys. Rev. A **35**, 5233 (1987).
[8] C. Tang, Phys. Rev. A **31**, 1977 (1985).
[9] J. Szépm, J. Cserti, and J. Kertész, J. Phys. A **18**, L413 (1985).
[10] J.-P. Eckmann, P. Meakin, I. Procaccia, and R. Zeitak, Phys. Rev. A **39**, 3185 (1989).
[11] J.-P. Eckmann, P. Meakin, I. Procaccia, and R. Zeitak, Phys. Rev. Lett. **65**, 52 (1990).
[12] R. Cafiero, L. Pietronero, and A. Vespignani, Phys. Rev. Lett. **70**, 3939 (1993).
[13] R.C. Ball, R.M. Brady, G. Rossi, and B.R. Thompson, Phys. Rev. Lett. **55**, 1406 (1985).
[14] R.C. Ball, Physica A **140**, 62 (1986).
[15] T.A. Witten and L.M. Sander, Phys. Rev. B **27**, 5686 (1983).
[16] T. Vicsek, Phys. Rev. Lett. **53**, 2281 (1984).
[17] L.P. Kadanoff, J. Stat. Phys. **39**, 267 (1985).
[18] J. Kertész and T. Vicsek, J. Phys. A **19**, L257 (1986).
[19] M.B. Hastings and L.S. Levitov, Physica D **116**, 244 (1998).
[20] M.B. Hastings, Phys. Rev. E **55**, 135 (1997).
[21] B. Davidovitch, H.G.E. Hentschel, Z. Olami, I. Procaccia, L.M. Sander, and E. Somfai, Phys. Rev. E **59**, 1368 (1999).
[22] B. Davidovich and I. Procaccia, Europhys. Lett. **48**, 547 (1999).
[23] B. Davidovich, M.J. Feigenbaum, H.G.E. Hentschel, and I. Procaccia, Phys. Rev. E **62**, 1706 (2000).
[24] B. Davidovich and I. Procaccia, Phys. Rev. Lett. **85**, 3608 (2000).
[25] E. Somfai, L.M. Sander, and R.C. Ball, Phys. Rev. Lett. **83**, 5523 (1999).
[26] T.C. Halsey, Phys. Rev. Lett. **59**, 2067 (1987).
[27] W.W. Mullins and R.F. Sekerka, J. Appl. Phys. **34**, 323 (1963).
[28] Y. Couder, F. Argoul, A. Arnéodo, J. Maurer, and M. Rabaud, Phys. Rev. A **42**, 3499 (1990).